NEW DIFFRACTION DATA

Crystal structure of haloxon, $C_{14}H_{14}Cl_3O_6P$

James A. Kaduk [1,2,a)] Stacy Gates-Rector [3] and Thomas N. Blanton [3]
[1]*Illinois Institute of Technology, 3101 S. Dearborn St., Chicago, IL 60616, USA*
[2]*North Central College, 131 S. Loomis St., Naperville, IL 60540, USA*
[3]*ICDD, 12 Campus Blvd., Newtown Square, PA 19073-3273, USA*

The crystal structure of haloxon has been solved and refined using synchrotron X-ray powder diffraction data, and optimized using density functional theory techniques. Haloxon crystallizes in space group $P2_1/n$ (#14) with $a = 19.60382(6)$, $b = 10.05473(3)$, $c = 8.73591(2)$ Å, $\beta = 92.6617(2)°$, $V = 1720.088(11)$ Å^3, and $Z = 4$. The structure consists of discrete molecules. The mean planes of the fused ring systems are approximately 0–11 and 011. The rings form staggered stacks perpendicular to these planes. There are no traditional hydrogen bonds in the structure, but several C–H···O and C–H···Cl hydrogen bonds contribute to the crystal energy. The powder pattern has been submitted to ICDD for inclusion in the Powder Diffraction File™ (PDF®). © *The Author(s), 2022. Published by Cambridge University Press on behalf of International Centre for Diffraction Data. This is an Open Access article, distributed under the terms of the Creative Commons Attribution licence (http://creativecommons.org/licenses/by/4.0/), which permits unrestricted re-use, distribution and reproduction, provided the original article is properly cited.* [doi:10.1017/S0885715622000422]

Key words: haloxon, Galloxon, powder diffraction, Rietveld refinement, density functional theory

I. INTRODUCTION

Haloxon (sold under the brand names Galloxon, Loxon, and Luxon among others) is an anthelminthic agent used in veterinary medicine to treat cattle. Haloxon is an antiparasitic drug that kills parasitic worms (helminths) and other internal parasites without causing significant damage to the host. The systematic name (CAS Registry Number 321-55-1) is bis(2-chloroethyl) (3-chloro-4-methyl-2-oxochromen-7-yl) phosphate. A two-dimensional molecular diagram is shown in Figure 1.

Haloxon was first mentioned by Brown *et al.* (1962). Several secondary sources indicate a Belgian patent BE610896, to Cooper, McDougall and Robertson, but we have been unable to obtain a copy, and are not aware of any published X-ray powder diffraction data on haloxon.

This work was carried out as part of a project (Kaduk *et al.*, 2014) to determine the crystal structures of large-volume commercial pharmaceuticals, and include high-quality powder diffraction data for them in the Powder Diffraction File (Gates-Rector and Blanton, 2019).
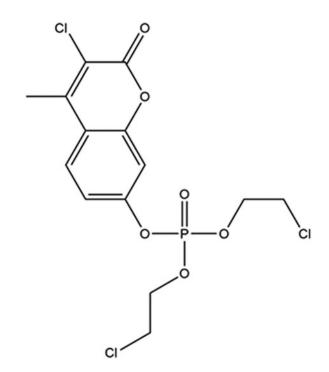
II. EXPERIMENTAL

Haloxon was a commercial reagent, purchased from Sigma (Lot #BO2641881), and was used as-received. The white powder was packed into a 1.5 mm diameter Kapton capillary and rotated during the measurement at ~50 Hz. The powder pattern was measured at 295 K at beamline 11-BM (Antao *et al.*, 2008; Lee *et al.*, 2008; Wang *et al.*, 2008) of the Advanced Photon Source at Argonne National Laboratory using a wavelength of 0.458963(2) Å from 0.5 to 50° 2θ with a step size of 0.009984375 and a counting time of 0.1 s per step. The high-resolution powder diffraction data were collected using twelve silicon crystal analyzers that allow for high angular resolution, high precision, and accurate peak positions. A silicon (NIST SRM 640c) and alumina (SRM 676a) standard (ratio Al_2O_3:Si = 2:1 by weight) was used to calibrate the instrument and refine the monochromatic wavelength used in the experiment.

The pattern was indexed, using N-TREOR (Altomare *et al.*, 2013), on a primitive monoclinic cell with $a = 19.62613$, $b = 10.05116$, $c = 8.73551$ Å, $\beta = 92.725°$, $V = 1721.3$ Å^3, and $Z = 4$. A reduced cell search in the Cambridge Structural Database (Groom *et al.*, 2016) with the chemistry H, C, Cl, O, and P only yielded no hits. The suggested space group was $P2_1/n$, which was confirmed by successful solution and refinement of the structure. The structure was solved by direct methods using EXPO2104 (Altomare *et al.*, 2013). Some of the atom types had to be reassigned manually.

Rietveld refinement was carried out using GSAS-II (Toby and Von Dreele, 2013). Only the 2.5–25.0° portion of the pattern was included in the refinement ($d_{min} = 1.060$ Å). All non-H bond distances and angles were subjected to restraints, based on a Mercury/Mogul Geometry Check (Bruno *et al.*, 2004; Sykes *et al.*, 2011). The Mogul average and standard deviation for each quantity were used as the restraint parameters. The restraints contributed 6.4% to the final χ^2. The hydrogen atoms were included in calculated positions, which were recalculated during the refinement using Materials Studio (Dassault, 2021). The three Cl atoms were refined anisotropically. The U_{iso} of the other heavy atoms were grouped by chemical similarity. The U_{iso} for the H atoms were fixed at 1.3× the U_{iso} of the heavy atoms to which they are attached. The peak profiles were described using the generalized microstrain model.

---
a)Author to whom correspondence should be addressed. Electronic mail: kaduk@polycrystallography.com

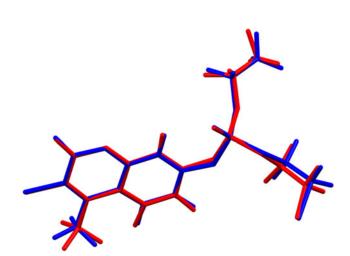Figure 1.   The 2D molecular structure of haloxon.

Figure 3.   Comparison of the Rietveld-refined (red) and VASP-optimized (blue) structures of haloxon. The rms Cartesian displacement is 0.135 Å. Image generated using Mercury (Macrae *et al.*, 2020).

The background was modeled using a 6-term shifted Chebyshev polynomial, and a peak at 6.28° 2θ to model the scattering from the Kapton capillary and any amorphous component.

The final refinement of 119 variables using 22 536 observations and 60 restraints yielded the residuals $R_{wp} = 0.0809$ and GOF = 1.74. The largest peak (0.32 Å from C19) and hole (1.87 Å from Cl2) in the difference Fourier map were 0.56(13) and $-0.48(13)$ $e\text{Å}^{-3}$, respectively. The largest errors in the difference plot (Figure 2) are in the shapes and

intensities of some of the strong low-angle peaks, and may indicate subtle changes in the specimen during the measurement.

The crystal structure was optimized using VASP (Kresse and Furthmüller, 1996) (fixed experimental unit cell) through the MedeA graphical interface (Materials Design, 2016). The calculation was carried out on 16 2.4 GHz processors (each with 4 GB RAM) of a 64-processor HP Proliant DL580 Generation 7 Linux cluster at North Central College. The calculation used the GGA-PBE functional, a plane wave cutoff energy of 400.0 eV, and a *k*-point spacing of 0.5 Å^{-1} leading to a $2 \times 2 \times 1$ mesh, and took ~21 h. A single-point density functional calculation (fixed experimental cell) and population analysis were carried out using CRYSTAL17 (Dovesi *et al.*, 2018). The basis sets for the H, C, and O atoms in the
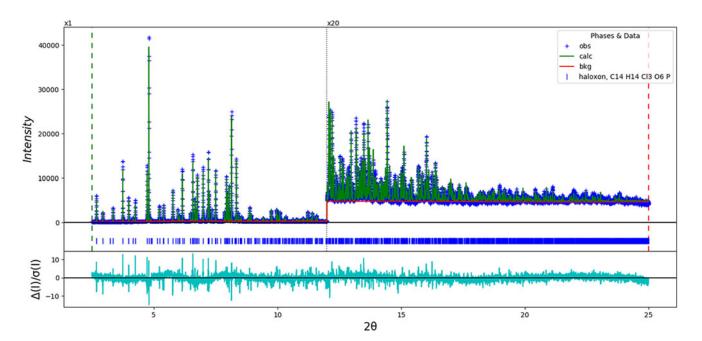

Figure 2.   The Rietveld plot for the refinement of haloxon. The blue crosses represent the observed data points, and the green line is the calculated pattern. The cyan curve is the normalized error plot. The vertical scale has been multiplied by a factor of 20× for 2θ >120°. The row of blue tick marks indicates the calculated reflection positions.
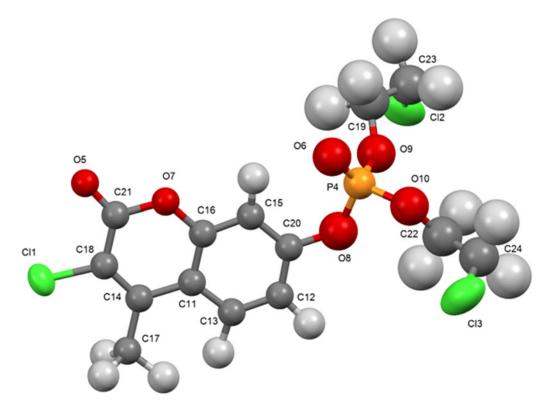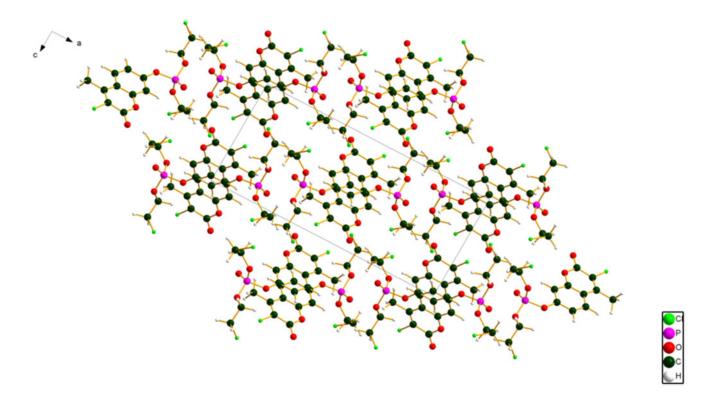
Figure 4.   The asymmetric unit of haloxon, with the atom numbering. The atoms are represented by 50% probability spheroids/ellipsoids. Image generated using Mercury (Macrae *et al.*, 2020).

calculation were those of Gatti *et al.* (1994), and those for P and Cl were that of Peintinger *et al.* (2013). The calculations were run on a 3.5 GHz PC using 8 *k*-points and the B3LYP functional, and took ~2.1 h.

III. RESULTS AND DISCUSSION

The root-mean-square (rms) Cartesian displacement between the Rietveld-refined and DFT-optimized structures of the haloxon molecule is 0.135 Å (Figure 3); the maximum
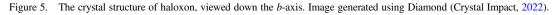

Figure 5.   The crystal structure of haloxon, viewed down the *b*-axis. Image generated using Diamond (Crystal Impact, 2022).

TABLE I. Hydrogen bonds (CRYSTAL17) in haloxon

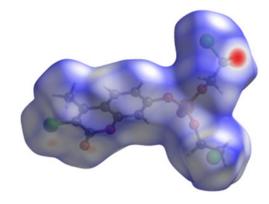| H-Bond	D-H (Å)	H···A (Å)	D···A (Å)	D-H···A (°)	Overlap (e)
C24–H37···O5	1.095	2.117	3.154	156.9	0.027
C15–H27···O6	1.088	2.313[a]	3.056	123.8	0.020
C19–H31···O5	1.099	2.491	3.402	139.3	0.014
C23–H36···O10	1.097	2.720	3.508	131.2	0.013
C22–H33···O6	1.101	2.586	3.498	139.6	0.012
C12–H25···Cl3	1.090	2.798	3.868	167.0	0.022
C17–H30···Cl2	1.097	2.880	3.950	165.1	0.016
C13–H26···Cl2	1.089	2.786	3.726	144.5	0.013
C17–H29···Cl1	1.096	2.651[a]	3.112	104.5	0.011
C19–H32···Cl2	1.098	2.817	3.684	135.8	0.010

[a]Intramolecular.

Figure 6. The Hirshfeld surface of haloxon. Intermolecular contacts longer than the sums of the van der Waals radii are colored blue, and contacts shorter than the sums of the radii are colored red. Contacts equal to the sums of radii are white.

difference is 0.353 Å at C24. The excellent agreement provides evidence that the refined structure is correct (van de Streek and Neumann, 2014). This discussion concentrates on the DFT-optimized structure. The asymmetric unit (with atom numbering) is illustrated in Figure 4. The best view of the crystal structure is down the *b*-axis (Figure 5). The structure consists of discrete molecules. The mean planes of the fused ring systems are approximately (0–11) and (011). The rings form staggered stacks perpendicular to these planes.

All of the bond distances, bond angles, and torsion angles fall within the normal ranges indicated by a Mercury/Mogul Geometry Check (Macrae *et al.*, 2020). Quantum chemical geometry optimization of the haloxon cation (DFT/B3LYP/6-31G*/water) using Spartan '18 (Wavefunction, 2020) indicated that the observed conformation is 3.6 kcal mol^{-1} higher in energy than the local minimum. The major differences (rms Cartesian displacement = 0.564 Å) occur at the chloromethyl and methyl groups. A conformational analysis (MMFF force field) indicates that the minimum-energy conformation is 1.5 kcal mol^{-1} lower in energy. The major difference is that the phosphate ester group is rotated by ∼180°; the molecule is thus fairly flexible. Although weak, the intermolecular interactions are important in determining the solid-state conformation.

Analysis of the contributions to the total crystal energy of the structure using the Forcite module of Materials Studio (Dassault, 2021) suggests that the intramolecular deformation energy is dominated by angle deformation terms, as might be expected in a molecule containing a fused ring system. The intermolecular energy is dominated by electrostatic attractions, which in this force field analysis also include hydrogen bonds. The hydrogen bonds are better analyzed using the results of the DFT calculation. There are no traditional hydrogen bonds in the structure (Table I), but several C–H···O and C–H···Cl hydrogen bonds contribute to the crystal energy.

The volume enclosed by the Hirshfeld surface of haloxon (Figure 6; Hirshfeld, 1977; Turner *et al.*, 2017) is 421.82 Å^3, 98.09% of 1/4 the unit cell volume. The packing density is thus fairly typical. The only significant-close contacts (red in Figure 6) involve the hydrogen bonds. The volume/non-hydrogen atom is 17.9 Å^3.

The Bravais–Friedel–Donnay–Harker (Bravais, 1866; Friedel, 1907; Donnay and Harker, 1937) morphology suggests that we might expect blocky morphology for haloxon, with perhaps {100} as major faces. A second-order spherical

harmonic model was included in the refinement. The texture index was 1.003(0), indicating that preferred orientation was slight in this rotated capillary specimen. The powder pattern of haloxon from this synchrotron dataset has been submitted to ICDD for inclusion in the Powder Diffraction File.

IV. DEPOSITED DATA

The Crystallographic Information Framework (CIF) files containing the results of the Rietveld refinement (including the raw data) and the DFT geometry optimization were deposited with the ICDD. The data can be requested at pdj@icdd.com.

CONFLICT OF INTEREST

The authors have no conflict of interest to declare.

Altomare, A., Cuocci, C., Giacovazzo, C., Moliterni, A., Rizzi, R., Corriero, N., and Falcicchio, A. (**2013**). "EXPO2013: a kit of tools for phasing crystal structures from powder data," J. Appl. Crystallogr. **46**, 1231–1235.

Antao, S. M., Hassan, I., Wang, J., Lee, P. L., and Toby, B. H. (**2008**). "State-of-the-art high-resolution powder X-ray diffraction (HRPXRD) illustrated with Rietveld refinement of quartz, sodalite, tremolite, and meionite," Can. Mineral. **46**, 1501–1509.

Bravais, A. (**1866**). *Etudes Cristallographiques* (Gauthier Villars, Paris).

Brown, N. C., Hollinshead, D. T., Kingsbury, P. A., and Malone, J. C. (**1962**). "A new class of compounds showing antihelmintic properties," Nature **194**, 379–379.

Bruno, I. J., Cole, J. C., Kessler, M., Luo, J., Motherwell, W. D. S., Purkis, L. H., Smith, B. R., Taylor, R., Cooper, R. I., Harris, S. E., and Orpen, A. G. (**2004**). "Retrieval of crystallographically-derived molecular geometry information," J. Chem. Inf. Sci. **44**, 2133–2144.

Crystal Impact - Dr. H. Putz & Dr. K. Brandenburg (**2022**). *Diamond - Crystal and Molecular Structure Visualization*. Kreuzherrenstr. 102, 53227 Bonn, Germany. Available at: https://www.crystalimpact.de/diamond.

Dassault Systèmes (**2021**). *Materials Studio 2021* (BIOVIA, San Diego, CA).

Donnay, J. D. H. and Harker, D. (**1937**). "A new law of crystal morphology extending the law of Bravais," Am. Mineral. **22**, 446–447.

Dovesi, R., Erba, A., Orlando, R., Zicovich-Wilson, C. M., Civalleri, B., Maschio, L., Rerat, M., Casassa, S., Baima Salustro, J., and Kirtman, B. (**2018**). "Quantum-mechanical condensed matter simulations with CRYSTAL," WIREs Comput. Mol. Sci. **8**, e1360.

Friedel, G. (**1907**). "Etudes sur la loi de Bravais," Bull. Soc. Fr. Mineral. **30**, 326–455.

Gates-Rector, S. and Blanton, T. (**2019**). "The Powder Diffraction File: a quality materials characterization database," Powd. Diffr. **39**(4), 352–360.

Gatti, C., Saunders, V. R., and Roetti, C. (**1994**). "Crystal-field effects on the topological properties of the electron-density in molecular crystals - the case of urea," J. Chem. Phys. **101**, 10686–10696.

Groom, C. R., Bruno, I. J., Lightfoot, M. P., and Ward, S. C. (**2016**). "The Cambridge Structural Database," Acta Crystallogr. Sect. B: Struct. Sci., Cryst. Eng. Mater. **72**, 171–179.

Hirshfeld, F. L. (**1977**). "Bonded-atom fragments for describing molecular charge densities," Theor. Chem. Acta **44**, 129–138.

Kaduk, J. A., Crowder, C. E., Zhong, K., Fawcett, T. G., and Suchomel, M. R. (**2014**). "Crystal structure of atomoxetine hydrochloride (Strattera), $C_{17}H_{22}NOCl$," Powd. Diffr. **29**(3), 269–273.

Kresse, G. and Furthmüller, J. (**1996**). "Efficiency of ab-initio total energy calculations for metals and semiconductors using a plane-wave basis set," Comput. Mater. Sci. **6**, 15–50.

Lee, P. L., Shu, D., Ramanathan, M., Preissner, C., Wang, J., Beno, M. A., Von Dreele, R. B., Ribaud, L., Kurtz, C., Antao, S. M., Jiao, X., and Toby, B. H. (**2008**). "A twelve-analyzer detector system for high-resolution powder diffraction," J. Synchrotron Radiat. **15**(5), 427–432.

Macrae, C. F., Sovago, I., Cottrell, S. J., Galek, P. T. A., McCabe, P., Pidcock, E., Platings, M., Shields, G. P., Stevens, J. S., Towler, M., and Wood, P. A. (**2020**). "*Mercury 4.0*: from visualization to design and prediction," J. Appl. Crystallogr. **53**, 226–235.

Materials Design (**2016**). *MedeA 2.20.4* (Materials Design Inc, Angel Fire, NM).

Peintinger, M. F., Vilela Oliveira, D., and Bredow, T. (**2013**). "Consistent Gaussian basis sets of triple-zeta valence with polarization quality for solid-state calculations," J. Comput. Chem. **34**, 451–459.

Sykes, R. A., McCabe, P., Allen, F. H., Battle, G. M., Bruno, I. J., and Wood, P. A. (**2011**). "New software for statistical analysis of Cambridge Structural Database data," J. Appl. Crystallogr. **44**, 882–886.

Toby, B. H. and Von Dreele, R. B. (**2013**). "GSAS II: the genesis of a modern open source all purpose crystallography software package," J. Appl. Crystallogr. **46**, 544–549.

Turner, M. J., McKinnon, J. J., Wolff, S. K., Grimwood, D. J., Spackman, P. R., Jayatilaka, D., and Spackman, M. A. (**2017**). *CrystalExplorer17* (University of Western Australia). Available at: http://hirshfeldsurface.net.

van de Streek, J. and Neumann, M. A. (**2014**). "Validation of molecular crystal structures from powder diffraction data with dispersion-corrected density functional theory (DFT-D)," Acta Crystallogr. Sect. B: Struct. Sci., Cryst. Eng. Mater. **70**(6), 1020–1032.

Wang, J., Toby, B. H., Lee, P. L., Ribaud, L., Antao, S. M., Kurtz, C., Ramanathan, M., Von Dreele, R. B., and Beno, M. A. (**2008**). "A dedicated powder diffraction beamline at the advanced photon source: commissioning and early operational results," Rev. Sci. Instrum. **79**, 085105.

Wavefunction, Inc. (**2020**). Spartan '18 Version 1.4.5, Wavefunction Inc., 18401 Von Karman Ave., Suite 370, Irvine, CA 92612.